Fizika Nizkikh Temperatur, 2009, v. 35, Nos. 8/9, p. 812–828

Magnetic-field-induced effects in the electronic structure of itinerant *d*- and *f*-metal systems

G.E. Grechnev

B. Verkin Institute for Low Temperature Physics and Engineering of the National Academy of Sciences of Ukraine
47 Lenin Ave., Kharkov 61103, Ukraine
E-mail: grechnev@ilt.kharkov.ua

Received February 17, 2009

A paramagnetic response of transition metals and itinerant *d*- and *f*-metal compounds in an external magnetic field is studied by employing *ab initio* full-potential LMTO method in the framework of the local spin density approximation. Within this method the anisotropy of magnetic susceptibility in hexagonal close-packed transition metals is evaluated for the first time. This anisotropy is owing to the orbital Van Vleck-like paramagnetic susceptibility, which is revealed to be substantial in transition metal systems due to hybridization effects in electronic structure. It is demonstrated, that compounds TiCo, Ni_3Al, YCo_2, $CeCo_2$, YNi_5, $LaNi_5$ and $CeNi_5$ are strong paramagnets close to the quantum critical point. For these systems the Stoner approximation underestimates the spin susceptibility, whereas the calculated field-induced spin moments provided a good description of the large paramagnetic susceptibilities and magnetovolume effects. It is revealed, that itinerant description of hybridized *f* electrons produces magnetic properties of $CeCo_2$, $CeNi_5$, UAl_3, UGa_3, USi_3 and UGe_3 compounds in close agreement with experiment. In the uranium UX_3 compounds the strong spin–orbit coupling together with hybridization effects give rise to peculiar magnetic states, where the field-induced spin moments are *antiparallel to the external field* and the magnetic response is dominated by the orbital contribution.

PACS: **71.20.–b** Electron density of states and band structure of crystalline solids;
71.20.Be Transition metals and alloys;
75.10.Lp Band and itinerant models.

Keywords: electronic structure, itinerant systems, spin susceptibility, orbital paramagnetism.

Introduction

The interaction between the external magnetic field and the electronic spin moment is usually the only interaction which is taken into account when one is interested in the magnetic susceptibility χ of transition metal (TM, or T hereafter) or itinerant *f*-metal (IFM) systems. However, the orbital moments in these systems are by no means negligible, and they are expected to contribute essentially to magnetic susceptibility. First principles calculations proved to be a useful tool in modeling of various physical properties, including magnetic ones, of transition metal systems. Nonetheless, it is still controversial whether the one-electron band theory within the local spin density approximation (LSDA) [1] or the generalized gradient approximation (GGA) [2] describes consistently the magnetic properties of TM and, particularly, IFM compounds, which are alternatively discussed in a number of papers within the models based on a localized character of *d* and *f* electrons (see, e.g., Refs. 3, 4 and references therein).

We have carried out *ab initio* calculations of the electronic structure and magnetic properties of transition metals and representative series of TM and IFM compounds. On the basis of a comparison of the experimental data on χ and the results of calculations, we analyzed the electronic states and interactions responsible for the magnetic properties of these systems. This comparison allowed to identify domains of applicability of our method for calculating the paramagnetic susceptibility of TM and IFM compounds. Also, in this paper the atomic volume effect on magnetic susceptibility was studied with the aim to shed more light on the nature of paramagnetism and electron–electron interactions in TM and IFM systems. It is expected that corresponding volume (or pressure) derivatives of χ are especially sensitive to the mechanism of these interactions.

Computational techniques

The calculation of magnetic susceptibility of metallic systems is a rather difficult problem in solid state physics [5–8]. From a relativistic treatment, based on the Dirac equation, the total susceptibility in the absence of spontaneous magnetic moment can be expressed as the sum ([5,6]):

$$\chi_{\text{tot}} = \chi_{\text{spin}} + \chi_{\text{orb}} + \chi_{\text{so}} + \chi_{\text{dia}} + \chi_{L}, \qquad (1)$$

where these terms correspond to the Pauli spin susceptibility, a generalization of the Van Vleck orbital paramagnetism, a contribution due to the spin–orbit coupling, the Langevin diamagnetism of closed shells (core electrons), and generalization of Landau conduction electrons diamagnetism, respectively.

The χ_{so} term is a relativistic correction to the susceptibility, and it has been shown [6,7], that χ_{so} is a higher order term as compared with χ_{spin} and χ_{orb}, and its value was estimated to be much smaller than the other two terms for transition metals (about few percents). Hence χ_{so} has been usually neglected in theoretical studies of magnetic susceptibility of transition metals [5,9–13].

In order to evaluate the various terms in Eq. (1), it was proposed in Refs. 5–7 to calculate the corresponding wave-vector dependent susceptibilities $\chi(q)$ by using a realistic band structure of some transition metals, and then taking the limit $q \to 0$ either analytically [5] or by numerical extrapolation [6,7]. Also the linear response formalism based on a Green's function technique was employed to calculate the spin [10,11,13] and orbital [13] magnetic susceptibilities in some transition metals. In these calculations the exchange enhancement of the Pauli spin susceptibility was taken into account within the Stoner model.

In the framework of the Stoner model the exchange-enhanced Pauli paramagnetic spin susceptibility χ_P can be written in the form:

$$\chi_{\text{ston}} = S\chi_P \equiv \mu_B^2 N(E_F)[1 - IN(E_F)]^{-1}, \qquad (2)$$

where $\chi_P = \mu_B^2 N(E_F)$, S is the Stoner enhancement factor. The Stoner integral I, describing the exchange-correlation interaction of the conduction electrons, can be expressed in terms of the calculated parameters of the electronic structure [14,15]:

$$I = 1/N(E_F)^2 \sum_{qll'} N_{ql}(E_F) J_{qll'} N_{ql'}(E_F). \qquad (3)$$

Here $N(E_F)$ is the total density of electronic states at the Fermi level E_F, $N_{ql}(E_F)$ is the partial density of states for atom q in the unit cell, $J_{qll'}$ are the local exchange integrals:

$$J_{ll'} = \int g(\rho(r))\phi_l(r)^2 \phi_{l'}(r)^2 \mathrm{d}r, \qquad (4)$$

where $\phi_l(r)$ are the partial wave functions, and $g(\rho(r))$ is a function of the electronic density [16]. More elaborated spin-polarized approach was proposed in Ref. 17 for the calculation of χ_{spin}, however the orbital contributions to χ_{tot} have not been evaluated in that work.

In the present paper we apply another approach, which has been successfully used in Refs. 8, 18 to calculate magnetic susceptibility of some TM and IFM systems, including even anisotropy of χ. This approach is based upon the *ab initio* full-potential linear muffin-tin orbital method (FP-LMTO) [18,19] within the local spin density approximation for the exchange-correlation effects [16]. The underlying Kohn–Sham equations are solved for a generic potential without any shape approximation, and the volume and crystal structure are the only input parameters to calculations of this kind.

The details of our method are given elsewhere [8,18,19], and here we mention only main features of the present implementation, which are different from other used FP-LMTO techniques. In the present calculations, the FP-LMTO basis set included the *s*, *p*, *d*, *f* orbitals for *f* metals, and *s*, *p*, *d* orbitals for all other elements within a single, fully hybridizing, energy panel [19].

All relativistic effects, including spin–orbit coupling, were incorporated, and the effect of an external magnetic field **B** was taken into account self-consistently at each iteration by means of the Zeeman term:

$$\hat{H}_Z = \mathbf{B} \cdot (2\hat{\mathbf{s}} + \hat{\mathbf{l}}), \qquad (5)$$

where $\hat{\mathbf{s}}$ is the spin operator and $\hat{\mathbf{l}}$ is the orbital angular momentum operator. By this way, the present approach allows to calculate *ab initio* the field-induced spin and orbital magnetic moments.

When the field induced spin and orbital magnetic moments are calculated, the corresponding volume magnetization can be evaluated, and the ratio between the magnetization and the field strength provides a susceptibility, which basically corresponds to χ_{spin} and χ_{orb} terms in Eq. (1). We should note, that within these self-consistent calculations the effect of the spin–orbit coupling upon the calculated field-induced magnetic moments is actually included *implicitly*, i.e., without calculations of a separate χ_{so} term in Eq. (1).

In the case of hexagonal or tetragonal crystal structure the components of magnetic susceptibility, $\chi_{\parallel}$ and $\chi_{\perp}$, can be derived from the magnetic moments obtained in an external field, applied parallel and perpendicular to the *c* axis, respectively. We have tested the linearity of the $M(B)$ dependence, where M is the magnetization, and found it quite linear for the fields 0.5–10 T. For external fields about 1 T, however, a huge number of *k* points

(about 100 K) were necessary to get the desired accuracy, and we actually used the field of 10 T for most calculations in order to reduce the number of k points used. The calculated total energies were well converged ($\sim 10^{-6}$ Ry) with respect to all parameters involved, such as k-space sampling and basis set truncation.

In the present work we did not calculate the diamagnetic contributions to the susceptibility coming from core and conduction electrons, which correspond to the $\chi_{\rm dia}$ and χ_L terms in Eq. (1). The Langevin contributions $\chi_{\rm dia}$ can be estimated based on results of Refs. 5, 20, 21 and appeared to be between free-atom and free-ionic diamagnetic susceptibilities. To calculate the Landau diamagnetic contribution χ_L is a considerably more difficult problem (see [5,22–24] and references therein). The free-electron Landau limit is often used for estimations, giving a χ_L^0 that equals $-1/3$ of the Pauli spin susceptibility, though for many systems this crude approximation was found not to provide even the correct order of magnitude of the diamagnetic susceptibility.

Beyond the free-electron limit, χ_L can be expressed qualitatively as inversely proportional to an average effective mass of conduction electrons, m^*. Therefore this contribution appears to be large for some nontransition metals and semimetals (graphite, beryllium, cadmium, bismuth) with small values of m^* [22,23,25,26]. For transition metal systems χ_L is usually assumed to be negligible in comparison to considerable paramagnetic contributions, due to the predominantly large effective masses m^*. On the other hand, it was shown [23,24] that the anomalous diamagnetism can originate from a tiny group of quasi-degenerate electronic states with small m^*, situated in the vicinity of the Fermi energy E_F and this contribution can be many times larger than the free-electron Landau estimation χ_L^0.

Magnetic susceptibility of cubic transition metals

We first inspect the accuracy of the present method by comparing experimental and theoretical data for the magnetic susceptibility of TMs. The calculated densities of electronic states (DOS) for a series of TMs belonging to successive groups of the Periodic Table are presented in Fig. 1. One can see, that due to the strong s, p–d hybridization the conduction bands of TMs are rather wide, and the valent d states can be considered as itinerant ones. This justifies the use of the proposed technique to evaluate magnetic susceptibility for TMs. The calculated paramagnetic contributions to χ of the cubic TMs are given in Table 1 together with the estimated Langevin diamagnetism of closed shells and the experimental data on magnetic susceptibility.

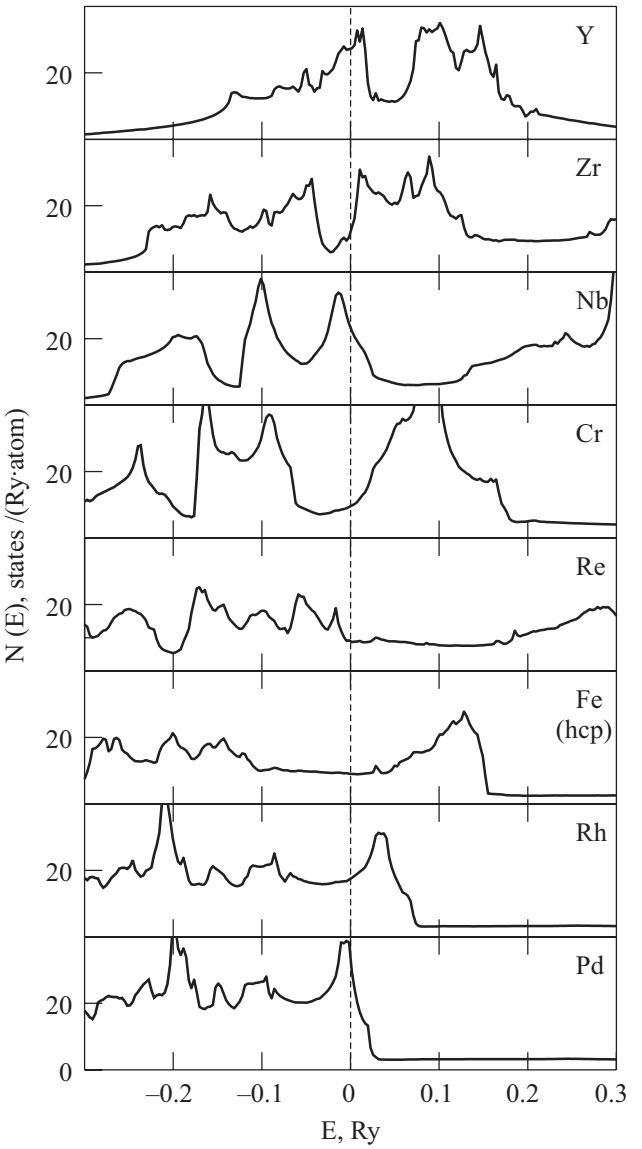

Fig. 1. Density of electronic states of transition metals: Y, Zr, Nb, Cr, Re, Fe (hcp), Rh, Pd. The Fermi level is marked with a vertical dashed line.

Table 1. Magnetic susceptibility of cubic transition metals

M	$\chi_{\rm ston}$	$\chi_{\rm spin}$	$\chi_{\rm orb}$	$\chi_{\rm dia}$ [20,21]	$\chi_{\rm spin}+\chi_{\rm orb}+\chi_{\rm dia}$	$\chi_{\rm exp}$ [27]	d ln χ / d ln V	
	10^{-6} emu/mol						theor	exp
V	180	175	113	–10	278	300	2.2	1.9 [28]
Nb	90	120	67	–10	177	212	1.9	1.7 [29]
Ta	82	90	45	–14	121	162	1.5	1.1 [29]
Cr	30	30	178	–15	193	180	2.1	2.0 [30]
Mo	21	23	92	–23	92	81	1.5	1.2 [31]
W	13	15	68	–36	47	53	0.5	0.5 [31]
Rh	71	75	65	–22	118	110	2.5	—
Ir	40	46	52	–50	48	30	2	—
Pd	481	587	119	–25	681	720	6	5.2 [28]
Pt	110	189	79	–40	228	220	2.8	—

The TMs of group VA — V, Nb, and Ta — have the bcc crystal lattice, and the Fermi level is situated within the descending part of a broad DOS $N(E)$ peak (see Fig. 1). As can be seen in Table 1, for these metals the orbital paramagnetic contributions χ_{orb} are very important since the spin contributions χ_{spin} alone are not sufficient to describe the experimental values of susceptibility. We note that the sum of calculated paramagnetic contributions appears to be lower than the experimental χ. This should be considered as rather expected underestimation for the LSDA ground state of group VA TMs. Due to the known over-bonding tendency of LSDA [19] the theoretical equilibrium volumes are about ~5% smaller than the experimental ones, and this resulted in slightly suppressed values of *ab initio* calculated χ_{spin} and χ_{orb}.

The TMs of the next group VIA — Cr, Mo and W — also have the bcc crystal lattice, and the Fermi level is positioned at the local DOS $N(E)$ minimum (see Fig. 1). In accordance with the low $N(E_F)$ values in these metals, the orbital paramagnetic contributions χ_{orb} are found to be substantially higher than the spin contributions. As is seen in Table 1, the calculated χ_{spin} and χ_{orb} appear to be in agreement with the experimental data on susceptibility. Obviously, the diamagnetic contributions χ_{dia} and χ_L have to be taken into account.

For the fcc transition metals of group VIIIA the Fermi level lies at a sharp DOS $N(E)$ peak, correspondingly below (Rh and Ir) and just after the peak (Pd and Pt). In Rh and Ir the calculated spin and orbital paramagnetic contributions are about the same size, and with additional diamagnetic contributions (χ_{dia} and χ_L) the good agreement with the experimental susceptibilities can be seen in Table 1. On the other hand, in Pd and Pt the high $N(E_F)$ values provide the substantially enhanced spin susceptibilities χ_{spin}. However, it should be noted that the orbital contribution χ_{orb} is needed to achieve a good agreement with the experiment.

One can see from Table 1 that the Stoner approach underestimates substantially the spin susceptibility in Pd and Pt. There is actually the general trend found also for other TMs that the Stoner model provides smaller values of the spin susceptibility χ_{ston}, comparatively to the field-induced calculated χ_{spin}. We should emphasize that *ab initio* LSDA calculations take into account the nonuniform induced magnetization density in the unit cell and presumably provide more accurate values of χ_{spin}.

Based on the calculated $\chi_{\text{spin}}(V)$ and $\chi_{\text{orb}}(V)$, the volume dependence of the magnetic susceptibility (VDMS) $\mathrm{d}\ln\chi/\mathrm{d}\ln V$ was evaluated and compared with the experimental data for the cubic TMs (see Table 1). The calculated large value of VDMS in Pd is in agreement with the experimental values of the pressure effect on χ [28] and also with the magnetostriction measurements for Pd [31]. For other cubic TMs the VDMS is smaller, $\mathrm{d}\ln\chi/\mathrm{d}\ln V \simeq 1$–2, and also is in agreement with the available experimental data. For the isovalent metals belonging to the same group of the Periodic Table one can notice from Table 1 that $\mathrm{d}\ln\chi/\mathrm{d}\ln V$ appears to decrease with increasing atomic number of the element, i.e., in the $3d \to 4d \to 5d$-metal series.

Magnetic susceptibility of hcp transition metals

In the present work the field-induced spin and orbital magnetic moments were also calculated for TMs which possess the hcp crystal structure at ambient pressure. The calculations were performed for varying atomic volume at the corresponding experimental lattice parameters ratios *c/a*. The averaged values of the calculated and experimental susceptibilities $\bar{\chi} = (\chi_{\parallel} + 2\chi_{\perp})/3$ and the anisotropies $\Delta\chi$ are listed in Table 2. Also the Langevin diamagnetic terms χ_{dia}, estimated according to Refs. 20, 21, and the calculated exchange-enhanced Pauli susceptibilities χ_{ston} are presented in the Table 2.

Table 2. Magnetic susceptibility of hcp transition metals

M	χ_{ston}	χ_{spin}	χ_{orb}	χ_{dia} [20,21]	$\chi_{\text{spin}}+\chi_{\text{orb}}+\chi_{\text{dia}}$	χ_{exp} [27]	$\Delta\chi_{\text{theor}}$	$\Delta\chi_{\text{exp}}$ [27]	$\mathrm{d}\ln\chi/\mathrm{d}\ln V$
	10^{-6} emu/mol								theor
Sc	207	267	38	–10	295	300	–5	–10	4
Y	163	191	26	–15	202	178	–8	–22	2
Lu	146	199	25	–20	204	193	–10	–25	2
Ti	42	61	73	–9	125	140	8	21	1.2
Zr	46.5	59	51	–10	100	120	10	51	0.2
Hf	31	37	39	–16	60	70	5	32	0.9
Re	25	34	77	–36	75	68	–4	–5	1.0
Ru	35	40	68	–23	85	50	–12	–9	1.9
Os	23.5	30	56	–44	42	20	–5	–5	1.7

As can be seen from Table 2, for trivalent TMs Sc, Y, and Lu the spin contributions to susceptibility χ_{spin} are substantially larger than Van Vleck orbital paramagnetism χ_{orb}. Also χ_{spin} is notably larger than the χ_{ston} susceptibilities which were calculated within the Stoner approximation (Eq. (2)). For these IIIA group TMs the sums of χ_{spin}, χ_{orb} and χ_{dia} appear to be in agreement with the corresponding experimental susceptibilities. Regarding the anisotropy of susceptibility, our calculations reproduce the sign and order of magnitude of $\Delta\chi$, and also a rise of $|\Delta\chi|$ in a the series Sc $\to$ Y $\to$ Lu (see Table 2).

For the IVA group TMs — Ti, Zr, and Hf — the calculated values of $\overline{\chi}$ are also in a qualitative agreement with experimental data, taking into account somewhat reduced $\chi_{\rm spin}$ and $\chi_{\rm orb}$ for the *theoretical* LSDA atomic volumes, as discussed above. The contributions $\chi_{\rm spin}$ and $\chi_{\rm orb}$ are about the same size indicating again the importance of the Van Vleck paramagnetism in TM. Also, in the case of Ti, Zr, and Hf the exchange enhanced Stoner susceptibility $\chi_{\rm ston}$ is about 20% lower than the field-induced calculated $\chi_{\rm spin}$.

It is seen in Table 2 that our calculations reproduce the positive sign of the anisotropy $\Delta\chi$ for the IVA group TMs, however, the calculated anisotropy appeared to be substantially lower than experimentally observed $\Delta\chi$ values. One should note that in these metals the Fermi level is situated close to the DOS $N(E)$ minimum, as can be seen in Fig. 1 for Zr. This implies the presence of the *sp–d* hybridized states with low effective masses, which can provide a notable anisotropic diamagnetic term χ_L, giving additional contribution to $\Delta\chi$. In the case of a complicated multiband structure of hcp transition metals it is not feasible to calculate correctly or even estimate the χ_L contribution, which can be responsible for the noted discrepancy with the experimental data on $\Delta\chi$.

In connection with this we can also assume that the difference between the calculated and experimental susceptibilities in the case of group VIIIA hcp transition metals Ru and Os (see Table 2) could arise from a substantial diamagnetic contribution χ_L. For these metals the calculated Van Vleck susceptibility $\chi_{\rm orb}$ is about twice as large as the $\chi_{\rm spin}$ term, and presumably this dominant $\chi_{\rm orb}$ contribution is the main source of the observed $\Delta\chi$, which is reproduced quite well by the calculations. This is also the case of the hcp Re, where a good agreement with the respective experimental data was obtained for the calculated $\overline{\chi}$ and $\Delta\chi$. Also, for Re, Ru and Os the field-induced calculated contribution $\chi_{\rm spin}$ is notably higher than the corresponding Stoner estimation $\chi_{\rm ston}$, calculated according to Eq. (2).

At ambient conditions all hcp transition metals have a c/a ratio close to the ideal value of $\sqrt{8/3} \approx 1.633$, but, as can be seen from Table 2, $\Delta\chi > 0$ for Ti, Zr, Hf, whereas for Sc, Y, Lu, Ru and Os we find that $\Delta\chi < 0$. This means that the c/a ratio is not the main factor determining the sign of $\Delta\chi$. In fact, the behavior of $\Delta\chi$ in hcp TMs is determined by a delicate balance between the Zeeman energy, exchange effects and the spin–orbit coupling. We emphasize that the sign and order of magnitude of $\Delta\chi$ are always reproduced for the hcp transition metals in the framework of our field-induced band structure calculations. As seen from Table 2, the sign of the experimental anisotropy of the magnetic susceptibility [27,32] is positive in Ti, Zr, and Hf (group IVA), but $\Delta\chi$ is negative in Sc, Y, Lu (group IIIA), Re (group VIIA), Ru and Os (group VIIIA). The absolute values of the calculated anisotropy are also in a qualitative agreement with the experiment, with allowance made for the observed [27,32] strong temperature dependence of $\Delta\chi$.

Magnetic properties of hcp iron

Recent *ab initio* total energy calculations for different crystal structures of iron, performed over a wide volume range, as well as the recent experimental studies with diamond anvil cells, have confirmed the stability of the hcp ground state at pressures above 15 GPa (see [33–35] and references therein). The hcp phase of iron is also expected for temperatures and pressures corresponding to the Earth's inner core conditions [35]. These calculations, however, have not provided a clear picture of magnetic properties of the hcp iron and their anisotropy.

Our spin polarized electronic structure calculations have not revealed a spontaneous magnetic moment for the hcp iron, and the absence of macroscopic magnetization is in agreement with the recent observation of the onset of superconductivity in iron at pressures 15 GPa < P < 30 GPa and below 2 K. On the other hand, the presence of magnetic fluctuations in the hcp Fe has been put forward as a possible origin of the superconductivity [34]. It has been demonstrated in previous sections that our calculations of magnetic susceptibility for TMs reproduce experiments at ambient conditions accurately enough, including the measured anisotropy of hcp transition metals. This provides the basis on which magnetic properties of the hcp iron can be studied *ab initio* over a wide volume range, from the superconducting state to the Earth's inner core conditions.

The field-induced magnetic moments of the hcp iron were calculated for a number of atomic volumes, corresponding to pressures from 20 to 350 GPa where the hcp phase is stable. The *c/a* axial ratio was taken equal to 1.59, which minimizes the total energy of the hcp iron [33] and conforms with recent experimental data. At these conditions Fe does not spontaneously order magnetically, and a small magnetic moment develops only in the presence of a magnetic field. The corresponding density of electronic states in hcp Fe, presented in Fig. 1, is very similar to the DOS of the isoelectronic metals Ru and Os, calculated at ambient conditions.

Our calculations demonstrate that for the hcp iron the induced spin moments are parallel to the orbital moments, in agreement with Hund's third rule. It is particularly remarkable that the spin contribution to χ is even smaller than the orbital contribution ($\chi_{\rm spin} \simeq 0.7\chi_{\rm orb}$) at pressures about 300 GPa. The averaged value of the susceptibility of hcp iron $\overline{\chi}$ is found to be ranging from $170\cdot10^{-6}$ emu/mol ($P = 350$ GPa) to $350\cdot10^{-6}$ emu/mol ($P = 50$ GPa). The evaluated VDMS $d\ln\chi/d\ln V$ is presented in Fig. 2 and appears to be consistent with the

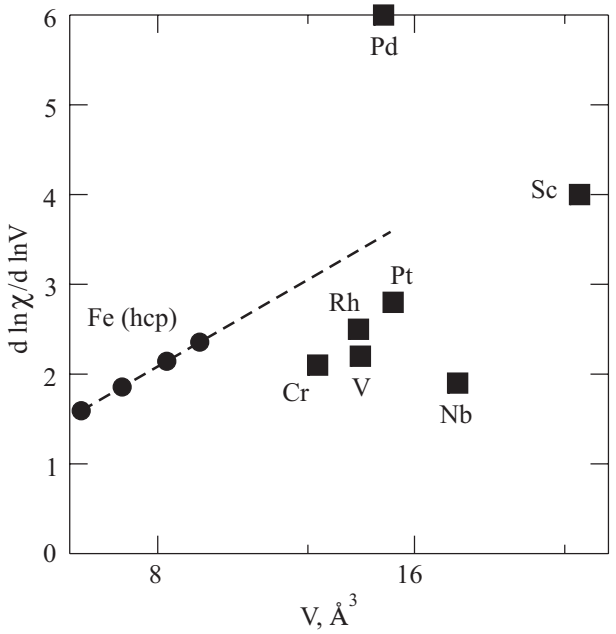

Fig. 2. Calculated volume dependence of the magnetic susceptibility $d\ln\chi / d\ln V$ for the hcp phase of iron (●, in a logarithmic scale) in the volume range corresponding to pressures from 350 to 50 GPa. The dashed line is a guide for the eye. The calculated for other transition metals $d\ln\chi / d\ln V$ at ambient pressure are presented for comparison (■, see also Tables 1 and 2).

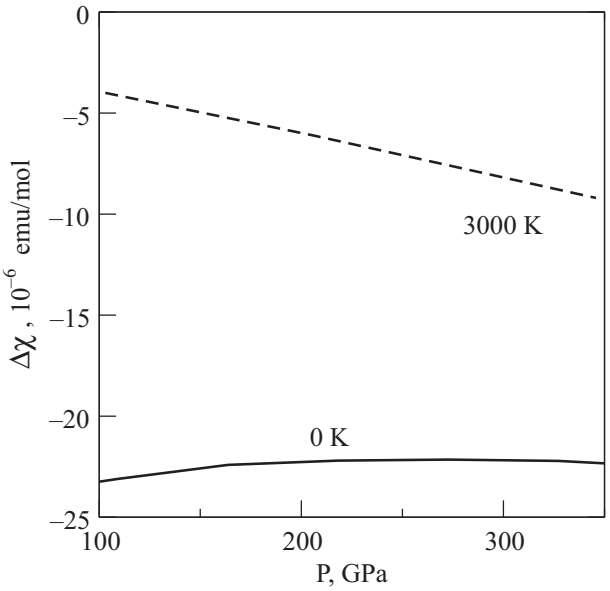

Fig. 3. Pressure dependence of the magnetic susceptibility anisotropy of the hcp iron. The solid and dashed lines correspond to the temperatures 0 and 3000 K, respectively.

calculated and experimental paramagnetostriction data for nonmagnetic transition metals. Based upon the calculated VDMS, the hcp iron occupies some intermediate position between Pd, which has strongly exchange-enhanced paramagnetism, and other TMs. For comparison, the Pauli spin contribution to the magnetic susceptibility was also calculated within the Stoner model (2) and appears to be in agreement with the field induced *spin* susceptibility, evaluated by using the full Zeeman term (5). The Stoner enhancement factor S was found to be about 3 for the hcp Fe at pressures of 20 GPa, which indicates on a possible role of spin-fluctuations as mediators of the superconductivity.

As expected, the anisotropy of χ comes almost exclusively from the orbital contribution χ_{orb}, which indicates that a relativistic treatment is necessary to explain magnetic properties even of comparatively «light» elements, like Fe. The calculated pressure and temperature dependencies of the magnetic susceptibility anisotropy of the hcp Fe are presented in Fig. 3. The thermal effects were taken into account through the Fermi–Dirac distribution function.

It has been demonstrated [8] that the observed seismic anisotropy of the Earth's inner core could have its origin in the anisotropy of the magnetic susceptibility of the hcp iron. A suggested mechanism of the seismic anisotropy of the Earth's inner core involves the anisotropy of the magnetic susceptibility of the hcp iron, and it is argued [8] that if χ is sufficiently anisotropic, a preferential orientation of the hcp crystals may occur. A validity of this mechanism is crucially dependent on the elastic anisotropy of the hcp iron, and with the calculated anisotropy of the elastic constants of the hcp Fe for $c/a = 1.59$ [33], the compressional velocity is faster along the c axis than along the a axis. Therefore, the present theoretical calculations demonstrate that the anisotropy of magnetic susceptibility of the hcp Fe can explain the seismological experiments.

Transition metal compounds with enhanced paramagnetic susceptibility

In the recent years the properties of the exchange-enhanced paramagnets and weak itinerant ferromagnets near magnetic instabilities has attracted substantial interest in connection with the so-called quantum critical points (QCP) [36,37]. The phase transitions in these QCP are due to nonthermal quantum fluctuations and take place at $T = 0$, though their influence can extend even at finite temperatures. The TM systems such as Pd, Sc, the hcp phase of Fe, TiCo, Ni_3Al, Ni_3Ga, $ZrZn_2$, $TiBe_2$, and MnSi compounds, a number of TCo_2 and TNi_5 alloys, and also some cerium and uranium based systems are close to QCP. Remarkably nonconventional properties were recently found in these materials, such as non-Fermi liquid behavior, metamagnetic transitions, unconventional superconductivity, co-existing with ferromagnetism in some cases. Though a number of theoretical models have been put forward [37], there is still no sufficient

understanding of these phenomena. Also the validity limits of band theory approaches and the LSDA approximation to the analysis of QCP phenomena have not been established.

In this section the fine details of electronic spectra and magnetic properties of systems close to QCP were studied by means of the filed-induced FP-LMTO calculations. Also, a detailed comparison with available experimental data has allowed to validate and tune up the quality of the band theory methods employed. Particular attention has been given to investigations of the magnetovolume effect in these systems in proximity of QCP.

TiCo, Ni_3Al *and* YCo_2 *systems*

The titanium compounds TiFe and TiNi were extensively studied for years in connection with a possibility to store hydrogen and the observation of the shape memory effect, respectively. TiCo, a compound with the intermediate band filling, has the same simple *B*2 cubic crystal structure (CsCl type) and exhibits a strong paramagnetism [36,38]. Also a transition to ferromagnetic (FM) state has been observed upon substitution of Ti with nontransition metals — Al and Ga [36,39]. This indicates itinerant character of the observed ferromagnetism in these alloys and proximity of TiCo to QCP.

Earlier band structure calculations have given controversial results, including a possibility of the FM phase in TiCo with a small magnetic moment $M \simeq 0.02\,\mu_B$ ([36,38] and references therein). According to the present calculations, TiCo exhibits a paramagnetic (PM) ground state and the corresponding density of electronic states is given in Fig. 4. The two groups of bands in the figure are formed by strong hybridization of *d* states of Ti and Co, and the Fermi level is situated above the pseudo-gap, in contrast to the TiFe compound.

The calculated contributions to magnetic susceptibility χ_{spin} and χ_{orb} are presented in Table 3. As seen in the table, the spin contribution χ_{spin} is large and dominant in TiCo, whereas the Stoner approach (2) provides substantially lower corresponding value of χ_{ston}. Taking also into account the Van Vleck contribution χ_{orb} we obtain very good agreement with the experimental susceptibility (see Table 3).

Table 3. Magnetic susceptibility of cubic compounds TiCo, Ni_3Al, YCo_2, $CeCo_2$

M	χston	χspin	χorb	χspin+χorb	χexp	d ln χ /d ln V	
	10^{-4} emu/mol					theor	exp
TiCo	7	10.5	2.7	13.2	13	6.4	5.4 [38]
YCo_2	12	15.5	2.5	18	20	12	15 [40]
$CeCo_2$	10	12	3	15	13	6	5 [41]
Ni_3Al	23	29.3	0.6	30	20*	7	3–7.7† [38]

*T = 293 K; †T = 100–300 K.

Note that the values of χ_{spin} and χ_{orb} in Table 3 are calculated at the theoretical lattice parameter *a*. As *a* increases and the system approaches QCP, a sharp rise of the contribution χ_{spin} determines the behavior of magnetic susceptibility, presented in Fig. 5. The corresponding calculated value of VDMS $d\ln\chi/d\ln V$ is listed in Table 3 and appears to be higher than in elemental TMs, including Pd and Sc (compare with the data in Tables 1 and 2). As seen in Table 3, the theoretical ground state

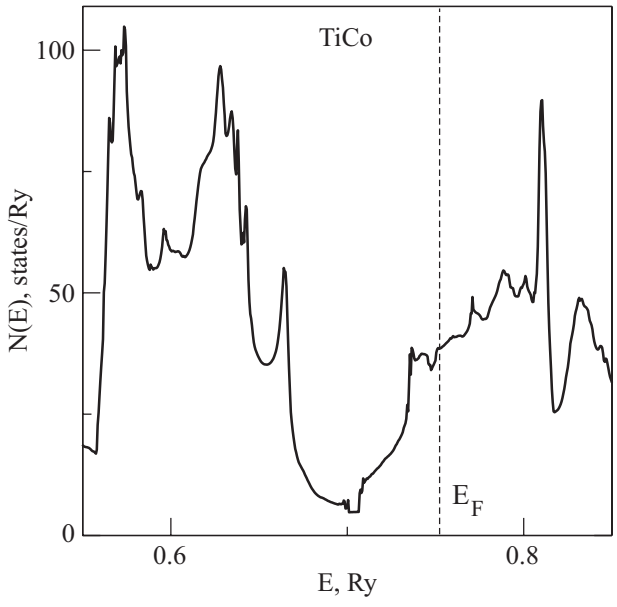

Fig. 4. Density of electronic states of TiCo. The Fermi level is marked by a vertical dashed line.

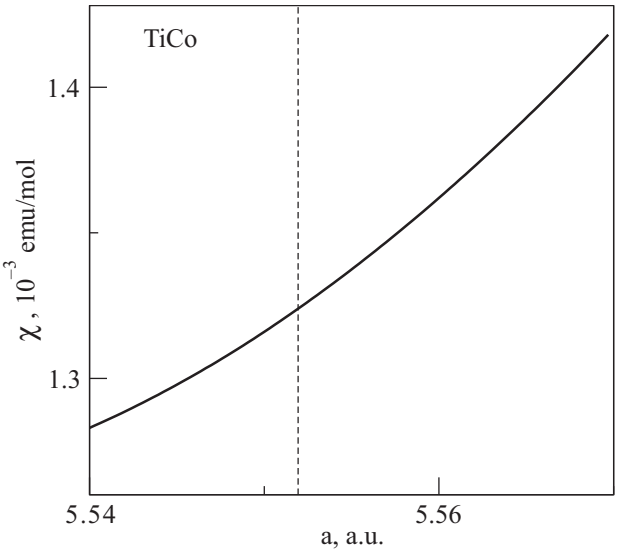

Fig. 5. The calculated magnetic susceptibility of TiCo as a function of the lattice parameter. The theoretical lattice parameter is marked by a vertical dashed line.

value of $d \ln \chi / d \ln V$ is in agreement with the experimental result of Ref. 38, obtained for TiCo at $T = 78$ K.

The intermetallic compound Ni_3Al has the cubic Cu_3Au-type structure, and it is widely used in air- and spacecraft technologies. At low temperatures Ni_3Al is an itinerant FM with the ordering temperature $T_C = 41$ K and the small magnetic moment about 0.2 μ_B [36,38]. Above T_C the magnetic susceptibility sharply decreases with temperature until at $T \simeq 300$ K it gradually falls into the region of χ typical for exchange-enhanced paramagnets (see Table 3). In addition to observed non-Fermi liquid transport properties under pressure and a transition to the PM phase at $P = 8.1$ GPa [42], strong pressure effects on magnetic susceptibility have been also detected in Ni_3Al [36,38].

The band structure of Ni_3Al calculated in the present work is found to be in good agreement with previous calculations (see Refs. 36, 38, 43). The calculated at the experimental lattice parameter total energy differences between the PM and FM phases are barely detectable, whereas in the close vicinity of the theoretical (LSDA) lattice parameter we get the PM ground state. The density of electronic states for the PM phase of Ni_3Al is given in Fig. 6. One can see the similarity of the $N(E)$ structure in Fig. 6 to that of the fcc palladium in Fig. 1. In fact this resemblance can be attributed to the moderate hybridization of d states of Ni with p states of Al in Ni_3Al, where the Fermi level is situated within the descending part of almost d character DOS peak with a high value of $N(E_F)$.

The paramagnetic contributions to susceptibility of Ni_3Al, χ_{spin} and χ_{orb} were calculated within FP-LMTO scheme for the PM phase in an external magnetic field and presented in Table 3. According to our calculations, at the equilibrium ground state volume of Ni_3Al the total energy of the FM phase is larger, but close to E_{total} of the PM phase. This makes the calculations of field-induced magnetic moments in Ni_3Al rather difficult, with a number of precautions exercised to get convergency, like increasing the number of k points used, and decreasing the external field value to 5 T. Moreover, the convergency was actually obtained for slightly reduced lattice parameters of Ni_3Al, $a \leq 0.98\, a_{theor}$, and we can consider the calculated χ_{spin} and χ_{orb} as approximations.

As seen in Table 3, the χ_{spin} contribution is definitely dominant in Ni_3Al, and it is substantially larger than the Stoner susceptibility value χ_{ston}, obtained according to Eq. (2). The agreement with the experimental data on χ and $d \ln \chi / d \ln V$ can be considered as satisfactory, taking into account the proximity of total energies for the FM and PM phases. This forced us to reduce the lattice parameters to get convergency of the field-induced calculations. Also it should be noted, that the experimental data for Ni_3Al in Table 3 were obtained for the most part at room temperatures, whereas the FP-LMTO calculations are done at $T = 0$ and apply to the ground state only.

The compound YCo_2 with the cubic Laves phase $C15$ structure is known as strongly enhanced Pauli paramagnet, which exhibits a distinct maximum in the temperature dependence of the magnetic susceptibility at $T \simeq 230$ K, and the itinerant metamagnetic transition to the FM phase in fields of about 70 T [36,44,45]. Also, a strong pressure effect on χ has been observed in YCo_2 and some $Y(Co_{1-x}M_x)_2$ alloys [40,45,46].

In order to find the origin of pronounced volume and temperature effects on magnetic susceptibility in YCo_2 compound, the volume dependent electronic structure was calculated *ab initio* by employing the FP-LMTO

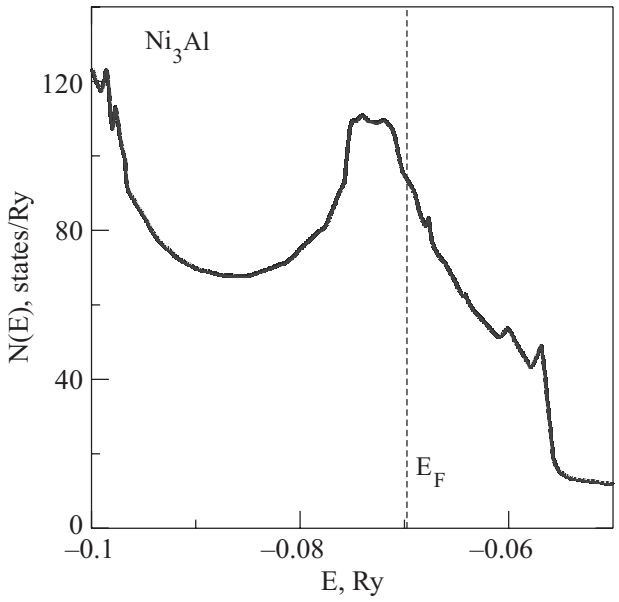

Fig. 6. Density of electronic states of Ni_3Al (PM phase). The Fermi level is marked by a vertical dashed line.

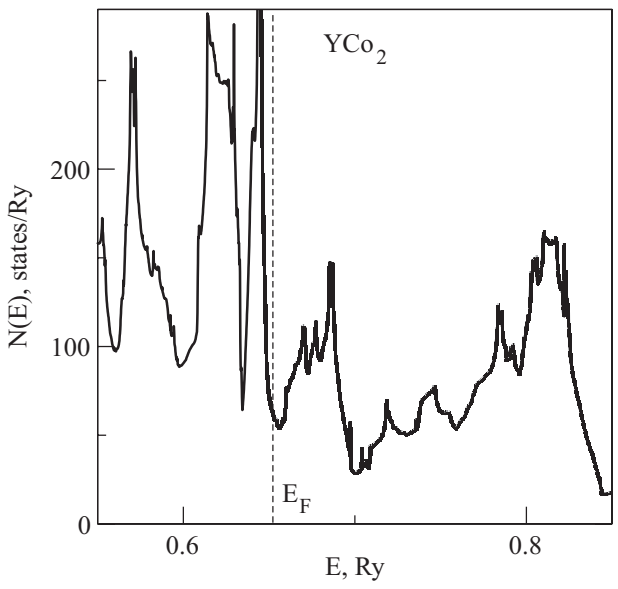

Fig. 7. Density of electronic states of YCo_2. The Fermi level is marked by a vertical dashed line.

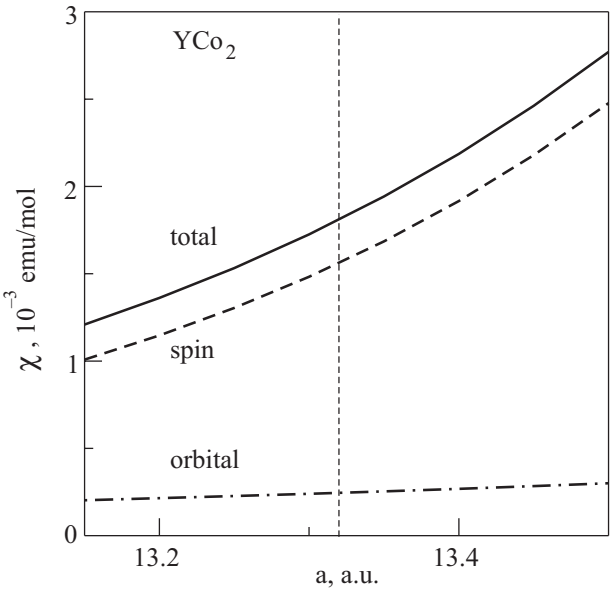

Fig. 8. The calculated contributions and total magnetic susceptibility of YCo_2 as a function of the lattice parameter. The theoretical lattice parameter is marked by a vertical dashed line.

method, within LSDA. According to our calculations, the PM phase is the ground state of the system. There is a pronounced hybridization of 3*d* states of Co with 4*d* states of Y, which provides a peculiar $N(E)$ structure at E_F (Fig. 7). The Fermi level is situated close to a local minimum of the DOS, just after a high and sharp DOS peak with the dominant *d* states of Co.

The spin and orbital contributions to the magnetic susceptibility were derived from the corresponding field-induced moments, which have been calculated at $T = 0$ in an external magnetic field of 10 T. These χ_{spin} and χ_{orb} contributions and the total paramagnetic susceptibility are presented in Fig. 8 and in Table 3. The main part of the strongly volume dependent spin contribution originates from the 3*d* states of Co, and these states are also responsible for the orbital Van Vleck contribution to χ. As seen in Fig. 8, as *a* increases and the system approaches QCP, a sharp rise of χ_{spin} determines the behavior of the magnetic susceptibility. The obtained very large value of magnetovolume effect in YCo_2, $\mathrm{d}\ln\chi/\mathrm{d}\ln V = 12$, appeared to be in agreement with the experimental data of Ref. 40 (15 ± 2).

YNi_5, $LaNi_5$ *and* $YNi_{5-x}Cu_x$ *systems*

Intermetallic compounds between nickel and trivalent TM (or rare earth R) elements of the RNi_5 type are distinguished by a great diversity of magnetic structures and properties [44]. For example, compounds with Y, La, Ce, and Lu are considered as the exchange-enhanced Pauli paramagnets, while $PrNi_5$ is a Van Vleck paramagnet. The compounds RNi_5 have a number of interesting physical properties, and they are used for making portable batteries. The compound $LaNi_5$ is promising for hydrogen storage, since the unit cell of this compound can store up to 7 hydrogen atoms. There are indications that substitution of some amount of nickel in RNi_5 compounds with other metals (Al, Co, Cr, Cu, Mn) alters their structural, electronic, and magnetic properties and can also improve their electrochemical characteristics [47]. In this work a detailed investigation of magnetic properties and electronic structure of RNi_5 (R = Y, La, Ce) compounds and $YNi_{5-x}Cu_x$ alloys was carried out by means of the first-principles calculations of their electronic structure and magnetic properties.

Ab initio calculations of the electronic structure were carried out for the RNi_5 compounds by employing the FP-LMTO method. These compounds crystallize in a hexagonal structure of the $CaCu_5$ type with six atoms per unit cell and two inequivalent types of transition metal atoms occupying positions of different symmetry (2*c* and 3*g* positions). The corresponding contributions to magnetic susceptibility were derived from the calculated field-induced moments in an external field of 10 T. In the FP-LMTO basis set the maximum value of the orbital quantum number *l* was taken as $l_{\max} = 2$ for Y, Ni, and Cu and by $l_{\max} = 3$ for La. The electronic structure calculations were performed for a number of lattice parameters close to the experimental one and the ratio *c/a* was fixed at its experimental value ($c/a \approx 0.8$ for RNi_5). The equilibrium lattice spacings a_{theor} and corresponding theoretical bulk moduli B_{theor} were determined from dependence of the total energy on the unit cell volume $E(V)$ by using the well known Murnaghan equation. The differences about 10% between the theoretical B_{theor} and experimental bulk moduli of RNi_5 are presumably related to the over-bonding tendency of the LSDA approach [19].

The electronic densities of states of RNi_5 calculated over a wide energy interval are presented in Fig. 9. The exchange-enhanced Pauli susceptibilities (2) for RNi_5 compounds were calculated in the framework of the Stoner model on the basis of the calculated densities of states at the Fermi level and the Stoner integrals (3). The results are presented in Table 4 and compared to the experiment. It is seen from the table that for YNi_5 and $LaNi_5$ the principal contribution to χ comes from the exchange-enhanced spin susceptibility. As a consequence of the large value of the Stoner enhancement factor for these compounds ($S \simeq 6$), small variations in $N(E_F)$ calculated by different methods will lead to noticeable differences in the calculated susceptibility χ_{ston}.

For YNi_5 and $LaNi_5$ the FP-LMTO method was used to calculate the induced spin and orbital magnetic moments in an external magnetic field, and the corresponding spin and orbital contributions to the susceptibility are listed in Table 4. As seen from the table, for these com-

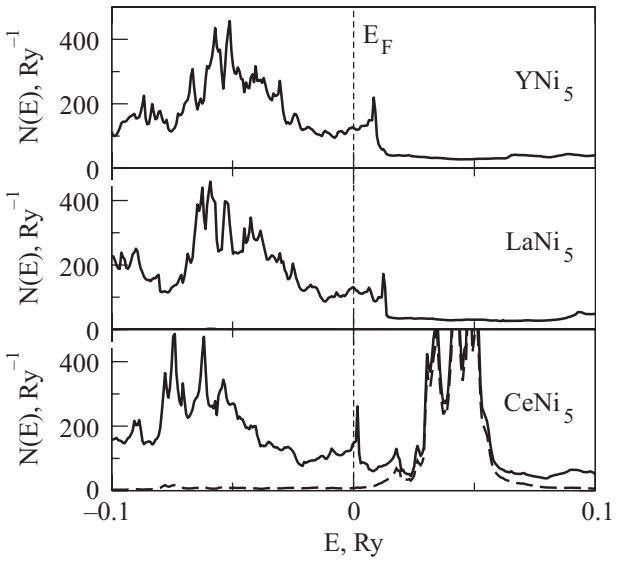

Fig. 9. Density of electronic states of RNi_5 compounds. The partial contributions of the *f* states are indicated by the dashed lines. The Fermi level is marked with a vertical dashed line.

pounds the spin contribution χ_{spin} is definitely dominant, but taking the Van Vleck contribution χ_{orb} into account provides almost complete agreement between the calculated and measured values of the susceptibility. Note that according to Refs. 20, 21, for RNi_5 compounds the absolute value of diamagnetic contribution to susceptibility from the ion core χ_{dia} amounts approximately to 3–4% of the sum of χ_{spin} and χ_{orb}.

Table 4. Magnetic susceptibility of compounds YNi_5, $LaNi_5$ and $CeNi_5$

M	χston	χspin	χorb	χspin+χorb	χexp	d ln χ / d ln V	
	10^{-3} emu/mol					theor	exp
YNi_5	1.5	1.78	0.23	2.0	1.9 [51,55]	7	6.6 [54]
$LaNi_5$	1.6	1.85	0.24	2.1	2.0 [52,53]	7.5	—
$CeNi_5$	1.6	2.39	0.62	3.0	3.0 [52,56]	4	3.9 [56]

It should be noted that earlier calculations [48,49] have given a spin-polarized ground state of the $LaNi_5$ system at the experimental values of the lattice parameters. In our FP-LMTO calculations in an external field of 10 T, the *theoretical* values of the lattice parameters of YNi_5, $LaNi_5$ and $CeNi_5$ were determined from the total energy considerations and appeared to be approximately 1% lower than the experimental values. A paramagnetic response was obtained for these compounds at the theoretical lattice parameters, with induced moments represented by the susceptibilities χ_{spin} and χ_{orb} in Table 4. At the *experimental* values of the lattice parameters we were unable to obtain stable induced moments in our calculations for these compounds. When the external field was «turned off», however, spontaneous spin polarization did not arise in YNi_5 and $LaNi_5$ systems during the self-consistent calculations of the electronic structure, in agreement with the experimental data [47,50–53]. The spontaneous spin polarization found in the calculations of Refs. 48, 49 for $LaNi_5$ is most likely due to insufficiently detailed calculations of the electronic structure under conditions where the system is close to magnetic instability.

The calculated volume derivatives of susceptibility d ln χ /d ln V are also listed in Table 4 and appear to be in agreement with the corresponding derivative resulted from the experimental studies of the pressure effect on χ for YNi_5 [54] at T = 77.3 K. According to these calculations the strongly volume dependent spin contribution to χ originates predominantly from the 3*d* states of Ni.

In Table 4 the values of induced magnetic moments M, calculated with the FP-LMTO method in the field of 4.8 T are listed together with the experimental moments, resulted from the polarized neutrons diffraction in YNi_5 at the same value of the external magnetic field [57]. The emphasis can be put on spin moments M_{spin} on the Y atom and in the interstitial area, which have opposite direction to the dominant spin moments of Ni. This is due to the inhomogeneous distribution of the spin density in the unit cell of YNi_5 because of hybridization of the electronic states of nickel and yttrium. The values of induced orbital moments M_{orb} are approximately the same on the atoms of Y and Ni, thus for yttrium M_{orb} is directed oppositely to M_{spin}. Here, presumably, one can see the certain analogy with the third Hund's rule for *f*-systems moments, as Y is situated at the beginning of the 4*d* period. Thus M_{spin} and M_{orb} are partly compensated, and resulting small moment on the atom of yttrium $M_{total} \simeq 0.4 \cdot 10^{-3} \mu_B$ appears to be below the precision level of the neutron experiments ($\pm 0.6 \cdot 10^{-3} \mu_B$ [57]). For the Ni atoms there is a good agreement of the calculated M_{total} with the experimental data [57]. In particular, the moments on the 3*g* sites appear to be larger than the moments on 2*c* sites. As it follows from Table 5, for YNi_5 one can observe a good agreement between the experimental magnetic susceptibility, the calculated value of χ, and also the neutron data on $\chi(n)$, obtained in external magnetic field [57].

It has been observed [47] that with increasing copper concentration x in $YNi_{5-x}Cu_x$ alloys, their magnetic susceptibility varies nonmonotonically and reaches a maximum at $x \simeq 0.3$ (see Fig. 10). In general, the nonmagnetic copper impurity enhances the paramagnetism of $RNi_{5-x}Cu_x$ alloys in the region $0 < x < 1$. This effect is the most pronounced in alloys with cerium and less pronounced in alloys with lanthanum [47,55,56].

Table 5. YNi_5: Calculated and experimental [57] magnetic moments (in $10^{-3}\mu_B$), induced by magnetic field of 4.8 T, and corresponding magnetic susceptibilities

Atom	M_{spin}	M_{orb}	M_{total}	χ, 10^{-3} emu/mol
Y (1*a*)	–0.79	0.36	–0.43	–0.05
Ni (2*c*)	2.93	0.42	3.35	0.78
Ni (3*g*)	4.07	0.32	4.39	1.53
Interstitial	–1.05	—	–1.05	–0.12
YNi_5	16.23	2.16	18.39	2.14
Neutron data				
Ni (2*c*)			2.4 ± 0.6	0.57 ± 0.09
Ni (3*g*)			4.1 ± 0.8	1.43 ± 0.20
Ni (tot)			17.1 ± 2.6	2.0 ± 0.3
[57]				2.0 ± 0.1

The presence of a peak in $N(E)$ slightly above the Fermi level in the RNi_5 compounds (see Fig. 9) suggests, that as nickel is substituted by copper in these compounds and the 3*d* band is filled, the Fermi level will shift into the region of the local maximum of $N(E)$, and one will therefore expect an increase of the Pauli spin susceptibility. However, in a quantitative analysis of this effect one must take into account that in alloys the fine structure of the DOS $N(E)$ should be smeared on account of impurity scattering of conduction electrons. In Ref. 55 the behavior of χ_{ston} (2) in $YNi_{5-x}Cu_x$ alloys has been calculated by taking into account the smearing on $N(E)$. However, the use of Lorentz function with the damping parameter Γ and, alternatively, a so-called «effective temperature» T^* within the Fermi–Dirac distribution function have not provided reasonable description of the experimental $\chi(x)$.

For more rigorous calculations of the density of states and spin susceptibility of the alloys we have used the KKR-ASA Green-function method in the coherent potential approximation (CPA) (details of the KKR-ASA-CPA method employed are presented in Ref. 58). In the self-consistent LSDA calculations by the CPA method a random distribution of Ni and Cu atoms in the 2*c* and 3*g* positions of the unit cell of the $CaCu_5$ crystal lattice was assumed. The CPA calculations give maxima of the local DOS $N_{Ni}(E_F)$ for the nickel atoms in the 2*c* and 3*g* sites at $x \simeq 0.5$ (Fig. 11), leading to growth of the Stoner parameter *I* according to Eq. (3). Here, as seen in Fig. 11, the total DOS $N(E_F, x)$ turns out to be practically constant in the interval $0 \le x \le 0.5$ owing to the competition between the contributions $N_{Ni}(E_F)$ and $N_{Cu}(E_F)$.

The magnetic susceptibility $\chi(x)$ of $YNi_{5-x}Cu_x$ alloys was evaluated according to Eqs. (2) and (3) with the use of the partial and total DOSs at the Fermi level, calculated with the KKR-ASA-CPA method (Fig. 11), and also the Stoner integrals *I*. As seen in Fig. 10, the results of this calculation are found in a qualitative agreement with the experimental data on χ. We note that the Van Vleck orbital contribution to the susceptibility χ_{orb} was not calculated in the framework of the KKR-ASA-CPA computa-

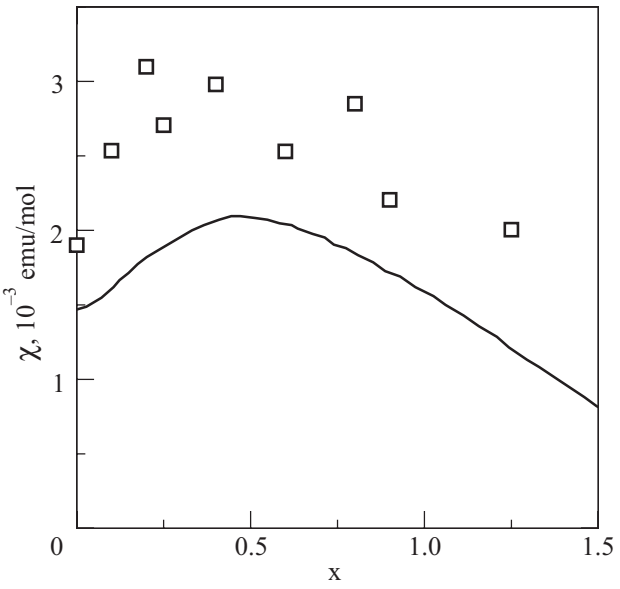

Fig. 10. Concentration dependence of the magnetic susceptibility of $YNi_{5-x}Cu_x$ alloys. □ — experimental data of Ref. 47. The solid curve corresponds to the KKR-ASA-CPA calculations.

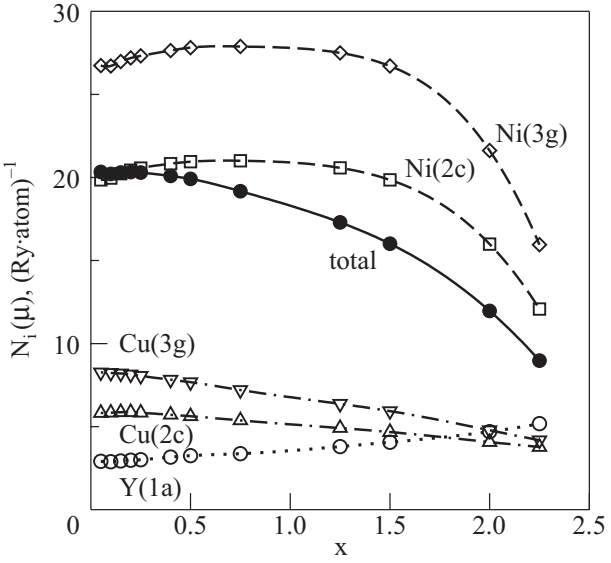

Fig. 11. Concentration dependence of the local densities of states at the chemical potential level in $YNi_{5-x}Cu_x$ alloys: for Ni atoms in the 2*c* (□) and 3*g* (◇) positions; for Cu in the 2*c* (△) and 3*g* (▽) positions; for Y in the 1*a* position (○), calculated by the KKR-ASA-CPA method. The corresponding total density of states (per atom) is represented by the solid curve (●).

tional scheme, and the value of χ_{orb} obtained for the compound YNi_5 ($0.23 \cdot 10^{-3}$ emu/mol; see Table 4) only improves the agreement with the experiment. On the whole, the results of KKR-ASA-CPA calculations of $\chi(x)$ are in agreement with the experiment for $YNi_{5-x}Cu_x$ alloys.

Itinerant *f*-metal compounds

Magnetism of the itinerant *f*-electron systems, including cerium and uranium compounds, the strength of related electronic correlations and the problem of localization–delocalization are matters of a long standing considerable interest. It is believed that band theory approaches, like LSDA and GGA, are not appropriate for analysis of magnetism in *f* systems due to strong electron–electron correlations.

In this section we check whether the *ab initio* technique introduced above (the FP-LMTO method) can be used to describe magnetic properties of presumably itinerant *f*-metal compounds. The field-induced spin and orbital moments and the paramagnetic susceptibilities χ_{spin} and χ_{orb} were evaluated for a number of itinerant cerium and uranium systems and compared with the experimental data.

A pronounced pressure effect on χ has been recently observed in UX_3 compounds [18,59], and the corresponding VDMS derivatives $d \ln \chi / d \ln V$ were found to be almost temperature independent, except for UAl_3. We expect that the pressure derivative of magnetic susceptibility is especially sensitive to the nature of $5f$ electrons in these compounds. Therefore, a particular attention was given to investigations of the VDMS in *f* systems with competing spin and orbital magnetic moments.

$CeCo_2$ *and* $CeNi_5$ *systems*

Among the rare earth RCo_2 compounds with the cubic Laves phase lattice ($C15$), possessing rather complex magnetic structures and properties, $CeCo_2$ is regarded as an enhanced Pauli paramagnet. This compound shows superconductivity below $T_C \simeq 1.5$ K, often attributed to the Fulde–Ferrel–Larkin–Ovchinnikov mechanism, where the large Pauli susceptibility was proposed to play a leading role [41,44]. It is also believed that this compound shows evidence of the so-called intermediate valence behavior, which is presumably revealed in the anomalous equilibrium volumes trend in the series of $CeFe_2$, $CeCo_2$, and $CeNi_2$ [44,60]. In order to describe various properties of these CeM_2 compounds a number of theoretical models have been put forward, including Kondo-like models and mixed-valence models, which assume the cerium atom being in a state which is a mixture of the localized $4f^1$ and $4f^0$ configurations, resulting in a non-integer $4f$ occupation number (see Ref. 41 and references therein).

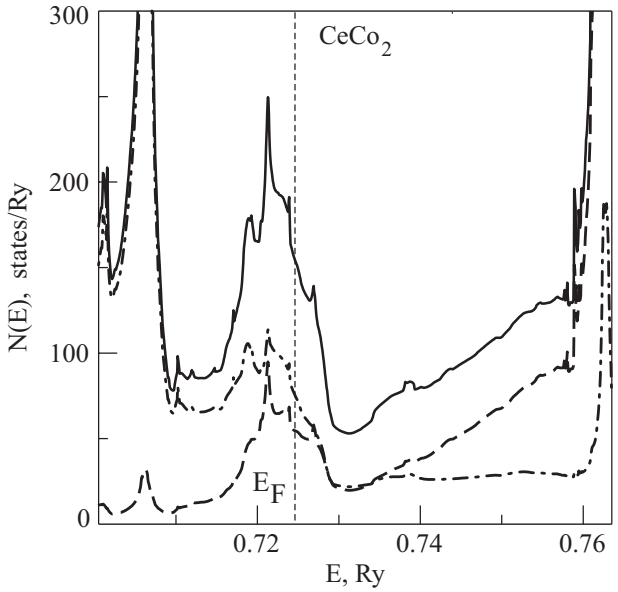

Fig. 12. Density of electronic states of $CeCo_2$. The total DOS and partial contributions of Ce *f* states, and Co *d* states are indicated by solid line, dashed line, and dashed-dotted line, respectively. The Fermi level is marked by a vertical dashed line.

Ab initio calculations of the electronic structure were performed for $CeCo_2$ by employing the full-potential LMTO method within LSDA, and the PM ground state with the $4f^0$ configuration of Ce was established. The DOS at the Fermi level comes mainly from the *f* electrons of Ce and the *d* electrons of Co (see Fig. 12), and the partial contributions of other states are substantially smaller. As a whole, the electronic structure at E_F is governed by a strong hybridization of the $4f$ (Ce) and $3d$ (Co) states, which leads to a filling of the bonding states, with the Fermi level located at the steep downward slope of a broad $N(E)$ peak, as distinct from YCo_2 (Fig. 7). The main part of the $4f$ and $5d$ states of Ce are situated higher in energy, and these hybridized states can be considered as the antibonding states.

The calculated spin and orbital contributions to the magnetic susceptibility of $CeCo_2$ are listed in Table 3. As seen in the table, the spin contribution χ_{spin} is the dominant one in $CeCo_2$, whereas the Stoner model (2) gives somewhat lower value of χ_{ston}. With the calculated Van Vleck contribution χ_{orb}, which amounts to about 25% of χ_{spin}, we have obtained a good agreement with the experimental susceptibility (see Table 3). The evaluated value of VDMS $d \ln \chi / d \ln V$ is also given in Table 3 and appears to be in a nice agreement with the experimental data of Ref. 41, obtained for $CeCo_2$ at $T = 78$ K.

Basically, the $CeCo_2$ compound with potentially strong electron correlations can be described with the

model of itinerant 4f states, which comes up naturally in the framework of electronic structure calculations performed within LSDA. It is shown that magnetic properties of $CeCo_2$, including magnetovolume effect, can be explained within the theory of itinerant magnetism, assuming the hybridized 4f electrons and employing the FP-LMTO calculations of field-induced magnetic moments.

For the $CeNi_5$ compound *ab initio* calculations of the electronic structure were carried out by employing the FP-LMTO method exactly like in the previous sections. The maximum value of the orbital quantum number l was taken as $l_{max} = 2$ for Ni and by $l_{max} = 3$ for Ce. The electronic density of states of $CeNi_5$ calculated over a wide energy interval is presented in Fig. 9, where the total DOS $N(E)$ is shown together with the partial contribution to DOS from the f states (dashed line). It is seen in Fig. 9 that in $CeNi_5$ the f states lie in the immediate vicinity of E_F and play a substantial role in the formation of the fine structure of DOS $N(E)$. The experimentally observed magnetic susceptibility of $CeNi_5$ is noticeably higher than experimental χ of YNi_5 and $LaNi_5$ (see Table 4). One can note that for $CeNi_5$ the exchange-enhanced Stoner susceptibility χ_{ston}, obtained according to Eq. (2), is much lower than χ_{spin} and it can not explain the experimental χ.

The FP-LMTO method was also employed to calculate the induced spin and orbital magnetic moments in an external field, and the corresponding spin and orbital contributions to susceptibility of $CeNi_5$ are listed in Table 4. As seen from the table, for this compound the spin contribution χ_{spin} is obviously dominant, but the Van Vleck term χ_{orb}, which comes mainly from the electrons in the atomic sphere of Ce, amounts to about 20% of the total susceptibility (to be compared with 11% in YNi_5 and $LaNi_5$). The sum of the self-consistently calculated at the theoretical lattice parameter χ_{spin} and χ_{orb} contributions provides a perfect agreement with the experiment for $CeNi_5$ [47,52,55,56]. The calculated volume derivative of susceptibility $d \ln \chi / d \ln V$ is also listed in Table 4 and appears to be in agreement with the corresponding derivative from the experimental studies of the pressure effect on χ for $CeNi_5$ [56] at $T = 77.3$ K.

Therefore, it is shown that the magnetic properties of $CeNi_5$ (which one might erroneously assume to be strongly correlated) can in fact be described with the itinerant 4f states within LSDA. Specifically, the magnetic susceptibility of $CeNi_5$ and the magnetovolume effect can be well reproduced with the *ab initio* calculations of the field-induced magnetic moments.

For $CeNi_{5-x}Cu_x$ alloys, unlike the systems $YNi_{5-x}Cu_x$ and $LaNi_{5-x}Cu_x$, a satisfactory description of the magnetic properties cannot be obtained in the LSDA approximation of band theory used in this study. This may be due to the appearance of the valence fluctuations of cerium in the $CeNi_{5-x}Cu_x$ alloys (see Ref. 56), the magnetic properties of which merit a separate detailed examination beyond the scope of this study.

USi_3, UGe_3, UAl_3 *and* UGa_3 *systems*

The uranium intermetallic compounds UX_3, where X is a nontransition element from the group-III or group-IV series (except for boron and carbon), crystallize in the cubic $AuCu_3$-type structure. The delocalization of f electrons in f systems and the related quenching of f-magnetic moment are usually attributed to either direct f–f overlap, or to the f–*spd* hybridization [61,62]. Since the U–U spacing in UX_3 compounds is far above the critical Hill limit [61,63], the direct 5f–5f interactions are weak, and these systems provide an exceptional opportunity to study the role of the f–*spd* hybridization in magnetic properties, ranging from Pauli-like paramagnetism (UAl_3, USi_3, UGe_3) and presumably itinerant antiferromagnetism (AFM) (UGa_3) to spin-fluctuation behavior (USn_3) and local-moment ordering (UIn_3, UTl_3, UPb_3 [18,61,62]).

The electronic structures of UX_3 compounds (X = Al, Ga, Si, Ge) were calculated by using the relativistic FP-LMTO method. The orbital polarization correction [64], corresponding to Hund's second rule, was also taken into account in the calculations. It is found that the main contributions to DOS at the Fermi level come from uranium 5f states and p states of ligand X, and a strong hybridization between these states provides narrow bands in the vicinity of E_F (see Figs. 13, 14 and 15). Although the Fermi level cuts the U $5f_{5/2}$ peak yielding a relatively

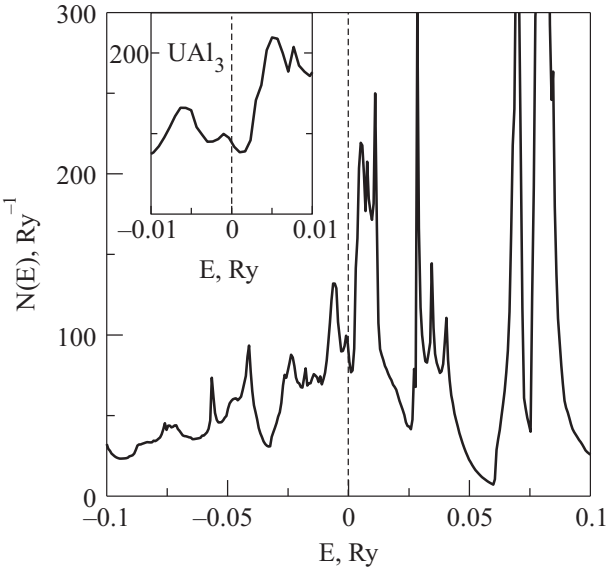

Fig. 13. Density of electronic states of UAl_3. Inset: The fine structure of $N(E)$ at E_F for UAl_3. The Fermi level positions (at 0 Ry) are marked by vertical lines.

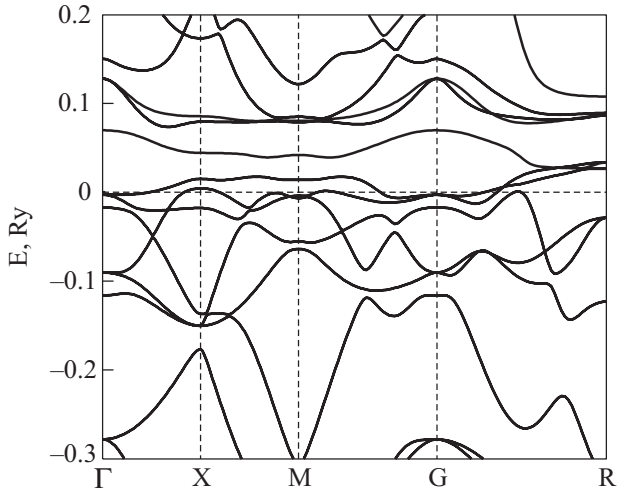

Fig. 14. Band structures of the PM phase of UGa_3. The Fermi level is marked by a horizontal dashed line.

high value of DOS at E_F, a pseudogap opens in the vicinity of E_F.

The calculated field-induced spin and orbital magnetic moments are found to be *antiparallel* in each studied UX_3 compound, in agreement with Hund's third rule. Also in these compounds the orbital Van Vleck contributions to magnetic susceptibility are substantially larger than the spin ones (see Table 6). Remarkably, these hybridization effects together with the spin–orbit coupling provide the peculiar magnetic states in the UX_3 compounds, where the spin moments are antiparallel to the applied field and the magnetic response is dominated by the orbital contribution. As can be seen in Table 6, the calculated induced moments appear to be in a good agreement with the experimental data on χ in UX_3.

Table 6. Magnetic susceptibility of UX_3 compounds

M	χ_{spin}	χ_{orb}	$\chi_{spin}+\chi_{orb}$	χ_{exp}	d lnχ /d lnV	
	10^{-4} emu/mol				theor	exp
UAl_3	–16	32	16	17	6	5.5 [59]
UGa_3	–25.5	46.5	21	20	6.3	5.3 [18]
USi_3	–1.5	7.4	5.9	5.8	3.9	2.5 [59]
UGe_3	–5.5	18.2	12.7	11	6.1	6.9 [59]

The calculated volume dependence of the magnetic susceptibility was found to be more pronounced for the orbital contribution to χ than for the spin contribution. Therefore, the large VDMS in UX_3, observed in Refs. 18, 59, is apparently related to the rapid quenching of the induced orbital moment with increasing width of the hybridized $5f$ band under applied pressure. As can be seen from Table 6, the volume derivatives of the field-induced moments are in a fair agreement with the corresponding experimental volume derivatives of the magnetic susceptibility. It should be noted that the significant temperature dependence of d ln χ /d ln V in UAl_3 [59] can be related to the fine structure of DOS at E_F (inset in Fig. 13) and a large volume effect on χ_{spin}.

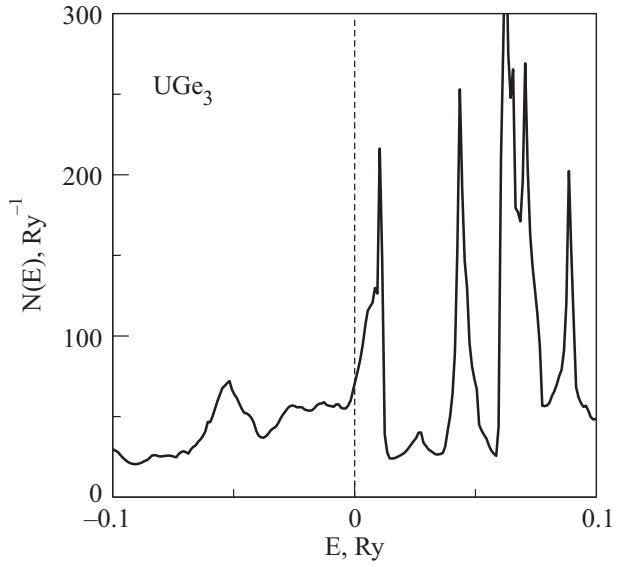

Fig. 15. Density of electronic states of UGe_3. The Fermi level is marked by a vertical dashed line.

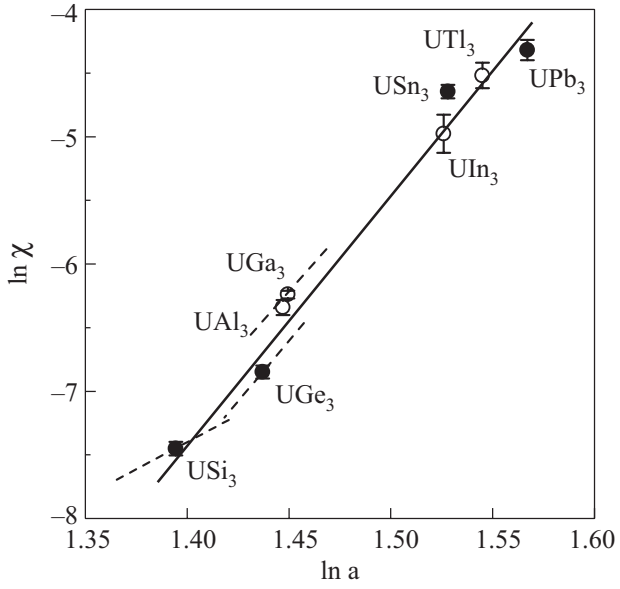

Fig. 16. Magnetic susceptibility of UX_3 systems versus lattice spacing (in a logarithmic scale), obtained by extrapolation of $\chi(T)$ from the paramagnetic phase (Refs. 18, 59, 61) to zero temperature. The dashed lines represent the calculated derivatives d ln χ /d ln V for UAl_3, UGa_3, USi_3, and UGe_3. The solid line is a guide for the eye.

As seen in Fig. 16, the values of d ln χ /d ln V for UX_3 follow a general trend in the dependence of magnetic susceptibility on the lattice parameter a. In particular, the behavior of the ln χ versus ln a in UX_3 compounds is close to linear with the slope corresponding to d ln χ /d ln $V \simeq 6$ (except USi_3). This trend allows to conclude that magnetic susceptibility of UX_3 is predominantly governed by the interatomic spacing variations.

For the itinerant AFM phase of UGa_3, observed below $T_N = 67$ K, the calculated spin and orbital magnetic moments appear to be antiparallel, very sensitive to atomic volume, and in a qualitative agreement with previous theoretical and neutron studies [18,65–67]. In general, the calculated AFM and field-induced magnetic moments are in a fair agreement with the experimental data, indicating the validity of the employed model of hybridized itinerant $5f$ states for the studied UX_3 compounds.

Conclusions

The novel technique for *ab initio* calculations of the electronic structure in external magnetic field was implemented within the density functional theory and the FP-LMTO method. In this way, the field-induced spin and orbital moments and the paramagnetic susceptibilities χ_{spin} and χ_{orb} were evaluated for a number of TM and IFM systems.

For transition metals the calculated susceptibilities and their volume dependencies d ln χ/d ln V appear to be in agreement with experiment. These metals are shown to possess substantial orbital contributions to the induced magnetization due to the hybridization of s, p and d states. It is demonstrated that the corresponding Van Vleck orbital contributions to magnetic susceptibility χ_{orb} are comparable or even higher than χ_{spin} in TM.

By means of the field-induced calculations for hcp transition metals, the anisotropy of magnetic susceptibility $\Delta\chi$ has been calculated for the first time. The sign and values of the calculated $\Delta\chi$ are in accordance with the experimental data at ambient conditions. The magnetic properties, including $\Delta\chi$, were evaluated for the high pressure hcp phase of Fe, which is expected to be the dominating element in the Earth's core. For the hcp iron the PM ground state with the substantial Stoner enhancement ($S \simeq 3$) is found in the region of the reported superconducting state (15 GPa < P < 30 GPa).

For the exchange-enhanced paramagnetic compounds TiCo, Ni_3Al, YCo_2, $CeCo_2$, YNi_5, $LaNi_5$ and $CeNi_5$, it is shown that the spin paramagnetism is dominant, while the Van Vleck orbital contribution to susceptibility amounts from about 10 up to 20% (TiCo, $CeCo_2$, $CeNi_5$) for these compounds. The Stoner approximation (2) is found to underestimate substantially the spin susceptibility, and within this approach, by using *ab initio* calculated $N(E_F)$ and integrals I, we were not able to explain the experimental susceptibilities and their volume dependencies in the studied TM compounds. On the other hand, the LSDA field-induced calculations take into account nonuniform induced magnetization density in the unit cell and provide more accurate values of χ_{spin}. Our method was able to describe the susceptibilities and VDMS in the strong paramagnetic compounds, which are close to quantum critical point.

Our calculations have revealed that the enhanced spin magnetic susceptibility in $YNi_{5-x}Cu_x$ alloys is extremely sensitive to the behavior of the partial contributions of Ni and Cu to the DOS at the Fermi level and also to nonuniform induced magnetization density at the Ni sites.

It is shown that itinerant picture of hybridized $4f$ electrons produces bulk and magnetic properties of $CeCo_2$ and $CeNi_5$ in close agreement with experiment. In general, the LSDA provides an adequate description of peculiar magnetic properties of the studied cerium compounds, including magnetovolume effects.

For the compounds UAl_3, UGa_3, USi_3 and UGe_3 the spin–orbit coupling appears sufficiently strong, and the field-induced spin and orbital moments are found to couple antiparallel, in accord with the Hund's third rule. In fact, the hybridization effects in UX_3 compounds give rise to peculiar magnetic states, where the spin moments are antiparallel to the field and the magnetic response is dominated by the orbital contribution. The good agreement of susceptibilities and their volume derivatives evaluated within LSDA with experimental data justifies the treatment of $5f$ states in UAl_3, UGa_3, USi_3 and UGe_3 compounds as the hybridized itinerant ones.

The author dedicates this work to the 90th anniversary of B.I. Verkin, who was one of pioneers in the field of magnetic properties studies in transition metals and compounds.

The author is grateful to O. Eriksson, P.A. Korzhavyi, A.S. Panfilov, I.V. Svechkarev, A. Grechnev and J.M. Wills for fruitful scientific discussions.

This work has been supported by the Russian-Ukrainian RFBR-NASU project 8-2009.

1. W. Kohn, *Rev. Mod. Phys*. **71**, 1253 (1999).
2. J.P. Perdew, K. Burke, and M. Ernzerhof, *Phys. Rev. Lett*. **77**, 3865 (1996).
3. V.Y. Irkhin and Y.P. Irkhin, *arXiv:Cond-mat/9812072v2,* 457 (1998).
4. V. Antonov, B. Harmon, and A. Yaresko, *Electronic Structure and Magneto-Optical Properties of Solids*, Kluwer Academic Publishers, N.Y. (2004).
5. J. Benkowitsch and H. Winter, *J. Phys. F: Met. Phys*. **13**, 991 (1983).
6. M. Yasui and M. Shimizu, *J. Phys. F: Met. Phys*. **15**, 2365 (1985).

7. M. Yasui, T. Takahashi, and J. Callaway, *J. Phys.: Condens. Matter* **3**, 2679 (1991).
8. G.E. Grechnev, R. Ahuja, and O. Eriksson, *Phys. Rev*. **B68**, 64414/1 (2003).
9. I. Bakonyi and H. Ebert, *J. Magn. Magn. Mater*. **89**, 350 (1990).
10. M. Matsumoto, J.B. Staunton, and P. Strange, *J. Phys.: Condens. Matter* **2**, 8365 (1990).
11. M. Matsumoto, J.B. Staunton, and P. Strange, *J. Phys.: Condens. Matter* **3**, 1453 (1991).
12. I. Bakonyi, H. Ebert, and A.I. Liechtenstein, *Phys. Rev*. **B48**, 7841 (1993).
13. M. Deng, H. Freyer, J. Voitlander, and H. Ebert, *J. Phys.: Condens. Matter* **13**, 8551 (2001).
14. L. Nordstrom, M.S.S. Brooks, and B. Johansson, *Phys. Rev*. **B46**, 3458 (1992).
15. K.H.J. Buschow, G.E. Grechnev, A. Hjelm, Y. Kasamatsu, A.S. Panfilov, and I.V. Svechkarev, *J. Alloys Compounds* **244**, 113 (1996).
16. U. von Barth and L. Hedin, *J. Phys. C: Solid State Phys*. **5**, 1629 (1972).
17. L.M. Sandratskii, *Adv. Phys*. **47**, 91 (1998).
18. G.E. Grechnev, A.S. Panfilov, I.V. Svechkarev, A. Delin, B. Johansson, J.M. Wills, and O. Eriksson, *J. Magn. Magn. Mater*. **192**, 137 (1999).
19. J.M. Wills, O. Eriksson, M. Alouani, and D.L. Price, *Full-Potential LMTO Total Energy and Force Calculations, in Electronic Structure and Physical Properties of Solids: The Uses of the LMTO Method*, H. Dreysse (ed.), Springer, Berlin (2000), p. 148.
20. P. Selwood, *Magnetochemistry,* Interscience, N.Y. (1956).
21. J. Banhart, H. Ebert, J. Voitlander, and H. Winter, *J. Magn. Magn. Mater*. **61**, 221 (1986).
22. G.E. Grechnev, I.V. Svechkarev, and Y.P. Sereda, *Sov. Phys. JETP* **75**, 993 (1978).
23. G.P. Mikitik and I.V. Svechkarev, *Fiz. Nizk. Temp*. **15**, 295 (1989) [*Sov. J. Low Temp. Phys*. **15**, 165 (1989)].
24. A.E. Baranovskiy, G.E. Grechnev, G.P. Mikitik, and I.V. Svechakarev, *Fiz. Nizk. Temp*. **29**, 473 (2003) [*Low Temp. Phys*. **29**, 356 (2003)].
25. G.E. Grechnev, J.W. McClure, and I.V. Svechkarev, *Fiz. Nizk. Temp*. **6**, 324 (1980) [*Sov. J. Low Temp. Phys*. **6**, 154 (1980)].
26. G.P. Mikitik and Y.V. Sharlai, *Fiz. Nizk. Temp*. **26**, 54 (2000) [*Low Temp. Phys*. **26**, 39 (2000)].
27. E.V. Galoshina, *Sov. Phys. Uspekhi* **17**, 345 (1974).
28. A.S. Panfilov, Y.Y. Pushkar', and I.V. Svechkarev, *Fiz. Nizk. Temp*. **14**, 532 (1988) [*Sov. J. Low Temp. Phys*. **14**, 293 (1988)].
29. E. Fawcett, *Phys. Rev*. **B2**, 1604 (1970).
30. I. Svechkarev and A. Panfilov, *Phys. Status Solidi* **B63**, 11 (1974).
31. E. Fawcett and V. Pluzhnikov, *Physica* **B119**, 161 (1983).
32. M.V. Volkenshtein, E.V. Galoshina, and T.N. Panikovskaya, *Sov. Phys. JETP* **70**, 730 (1975).
33. P. Söderlind, J.M. Moriarty, and J.M. Wills, *Phys. Rev*. **B53**, 14063 (1996).
34. I.I. Mazin, D.A. Papaconstantopoulos, and M.J. Mehl, *Phys. Rev*. **B65**, 100511/1 (2002).
35. G. Steinle-Neumann, R.E. Cohen, and L. Stixrude, *J. Phys.: Condens. Matter* **16**, S1109 (2004).
36. P.E. Brommer and J.J.M. Franse, *Strongly Enhanced Itinerant Intermetallics and Alloys,* in*: Handbook of Magnetic Materials*, K.H.J. Buschow (ed.), vol. 5, Elsevier, North Holland, Amsterdam (1990), p. 74.
37. S.M. Stishov, *Phys. Usp.* **47**, 789 (2004).
38. P.E. Brommer, G.E. Grechnev, J.J.M. Franse, A.S. Panfilov, Y.Y. Pushkar, and I.V. Svechkarev, *J. Phys.: Condens. Matter* **7**, 3173 (1995).
39. G.E. Grechnev and I.V. Svechkarev, *Fiz. Nizk. Temp*. **13**, 547 (1987) [*Sov. J. Low Temp. Phys*. **13**, 309 (1987)].
40. T. Goto and M.I. Bartashevich, *J. Phys.: Condens. Matter* **10**, 3625 (1998).
41. G.E. Grechnev, A.S. Panfilov, I.V. Svechkarev, A. Delin, B. Johansson, and J.M. Wills, *Physica* **B319**, 268 (2002).
42. P.G. Niklowitz, F. Beckers, G.G. Lonzarich, G. Knebel, B. Salce, J. Thomasson, N. Bernhoeft, D. Braithwaite, and J. Flouquet, *Phys. Rev*. **B72**, 024424/1 (2005).
43. D. Hackenbracht and J. Kübler, *J. Phys. F: Met. Phys.* **10**, 427 (1980).
44. J.J.M. Franse and R.J. Radwanski, *Magnetic Properties of Binary Rare-Earth 3d-Transition-Metal Intermetallic Compounds*, in: *Handbook of Magnetic Materials*, K.H.J. Buschow (ed.), vol. 7, Elsevier, North Holland, Amsterdam (1993), p. 194.
45. N.H. Duc and P.E. Brommer, *Formation of 3d-Moments and Spin Fluctuations in Some Rare-Earth-Cobalt Compounds*, in: *Handbook of Magnetic Materials*, K.H.J. Buschow (ed.), vol. 12, Elsevier, North Holland, Amsterdam (1999), p. 136.
46. A.E. Baranovskiy, G.E. Grechnev, A.S. Panfilov, I.V. Svechkarev, and O. Eriksson, *Phys. Techn. High Press*. **12**, 19 (2002).
47. A.G. Kuchin, A.S. Ermolenko, V.I. Khrabrov, G.M. Makarova, and E.V. Belozerov, *J. Magn. Magn. Mater*. **159**, 309 (1996).
48. H. Nakamura, D. Nguyen-Manh, and D.G. Pettifor, *J. Alloys Compounds* **281**, 81 (1998).
49. L.G. Hector, J.F. Herbst, and T.W. Capehart, *J. Alloys Compounds* **353**, 74 (2003).
50. D. Gignoux, F. Givord, R. Lemaire, and F. Tasset, *J. Less-Common Met*. **94**, 1 (1983).
51. E. Burzo, V. Pop, and I. Costina, *J. Magn. Magn. Mater*. **157**–**158**, 615 (1996).
52. M. Coldea, D. Andreica, M. Bitu, and V. Crisan, *J. Magn. Magn. Mater*. **157**–**158**, 627 (1996).
53. E. Burzo, S.G. Chiuzbaian, L. Chioncel, and M. Neumann, *J. Phys.: Condens. Matter* **12**, 5897 (2000).
54. G.E. Grechnev, A.V. Logosha, A.S. Panfilov, I.V. Svechkarev, and A.G. Kuchin, *Magnetovolume Effect in Exchange-Enhanced Itinerant Paramagnet* YNi_5, in: *Proceedings 7th International conference «Physical Phenomena in Solids»*, vol. 1, Kharkov's National University, Kharkov (2005), p. 111.

55. G.E. Grechnev, A.V. Logosha, I.V. Svechkarev, A.G. Kuchin, Yu.A. Kulikov, P.A. Korzhavyi, and O. Eriksson, *Fiz. Nizk. Temp*. **32**, 1498 (2006) [*Low Temp. Phys*. **32**, 1140 (2006)].
56. G. Grechnev et al., *arXiv:Cond-mat/0611325*, 5 (2006).
57. D. Gignoux, F. Givord, R. Lemaire, A. Nait-Saada, and A. Del-Moral, *J. Magn. Magn. Mater*. **23**, 274 (1981).
58. P.A. Korzhavyi, A.V. Ruban, I.A. Abrikosov, and H.L. Skriver, *Phys. Rev*. **B51**, 5773 (1995).
59. G.E. Grechnev, A.S. Panfilov, I.V. Svechkarev, A. Czopnik, A. Hackemer, D. Kaczorowski, and O. Eriksson, *Czech. J. Phys*. **54**, D359 (2004).
60. O. Eriksson, L. Nordstrom, M.S.S. Brooks, and B. Johansson, *Phys. Rev. Lett*. **60**, 2523 (1988).
61. V. Sechovsky and L. Havela, *Intermetallic Compounds of Actinides, in Ferromagnetic Materials*, K.H.J. Buschow (ed.), vol. 4, North Holland, Amsterdam (1988), p. 182.
62. M.R. Normann and D.D. Koelling, *Electronic Structure, Fermi Surfaces, and Superconductivity in f Electron Metals*, vol. 17, Elsevier, North Holland, Amsterdam (1993), p. 85.
63. T. Le Bihan, S. Heathman, S. Darracq, C. Abraham, J.-M. Winand, and U. Benedict, *High Temp. — High Press*. **27**/**28**, 157 (1996).
64. O. Eriksson, M.S.S. Brooks, and B. Johansson, *Phys. Rev*. **B41**, 7311 (1990).
65. A.L. Cornelius, A.J. Arko, J.L. Sarrao, J.D. Thompson, M.F. Hundley, C.H. Booth, N. Harrison, and P.N. Oppeneer, *Phys. Rev*. **B59**, 14473 (1999).
66. A. Hiess, F. Boudarot, S. Coad, P.J. Brown, P. Burlet, G.H. Lander, M.S.S. Brooks, D. Kaczorowski, A. Czopnik, and R. Troc, *Europhys. Lett*. **55**, 267 (2001).
67. M. Nakamura, Y. Koike, N. Metoki, K. Kakurai, Y. Haga, G.H. Lander, D. Aoki, and Y. Ōnuki, *J. Phys. Chem. Solids* **63**, 1193 (2002).